Original Article | Cardiovascular Imaging

eISSN 2005-8330
https://doi.org/10.3348/kjr.2025.0177
Korean J Radiol 2025;26(8):759-770

Korean Journal of Radiology
KJR

Impact of Deep Learning-Based Image Conversion on Fully Automated Coronary Artery Calcium Scoring Using Thin-Slice, Sharp-Kernel, Non-Gated, Low-Dose Chest CT Scans: A Multi-Center Study

Cherry Kim[1], Sehyun Hong[2], Hangseok Choi[3], Won-Seok Yoo[4], Jin Young Kim[5], Suyon Chang[6], Chan Ho Park[7], Su Jin Hong[8], Dong Hyun Yang[9], Hwan Seok Yong[10], Marly van Assen[11,12], Carlo N. De Cecco[12,13], Young Joo Suh[4]

[1]Department of Radiology, Korea University Ansan Hospital, Ansan, Republic of Korea
[2]Coreline Soft Co., Ltd, Seoul, Republic of Korea
[3]Medical Science Research Center, Korea University College of Medicine, Seoul, Republic of Korea
[4]Department of Radiology, Severance Hospital, Research Institute of Radiological Science, Yonsei University College of Medicine, Seoul, Republic of Korea
[5]Department of Radiology, Dongsan Hospital, Keimyung University College of Medicine, Daegu, Republic of Korea
[6]Department of Radiology, Seoul St. Mary's Hospital, College of Medicine, The Catholic University of Korea, Seoul, Republic of Korea
[7]Department of Radiology, Soonchunhyang University Cheonan Hospital, Cheonan, Republic of Korea
[8]Department of Radiology, Hanyang University Guri Hospital, Hanyang University College of Medicine, Guri, Republic of Korea
[9]Department of Radiology and Research Institute of Radiology, Cardiac Imaging Center, Asan Medical Center, University of Ulsan College of Medicine, Seoul, Republic of Korea
[10]Department of Radiology, Korea University Guro Hospital, Korea University College of Medicine, Seoul, Republic of Korea
[11]Department of Radiology and Imaging Sciences, Emory University School of Medicine, Atlanta, GA, USA
[12]Translational Laboratory for Cardiothoracic Imaging and Artificial Intelligence, Emory University School of Medicine, Atlanta, GA, USA
[13]Division of Cardiothoracic Imaging, Department of Radiology, Emory University, Atlanta, GA, USA

Objective: To evaluate the impact of deep learning-based image conversion on the accuracy of automated coronary artery calcium quantification using thin-slice, sharp-kernel, non-gated, low-dose chest computed tomography (LDCT) images collected from multiple institutions.

Materials and Methods: A total of 225 pairs of LDCT and calcium scoring CT (CSCT) images scanned at 120 kVp and acquired from the same patient within a 6-month interval were retrospectively collected from four institutions. Image conversion was performed for LDCT images using proprietary software programs to simulate conventional CSCT. This process included 1) deep learning-based kernel conversion of low-dose, high-frequency, sharp kernels to simulate standard-dose, low-frequency kernels, and 2) thickness conversion using the raysum method to convert 1-mm or 1.25-mm thickness images to 3-mm thickness. Automated Agaston scoring was conducted on the LDCT scans before (LDCT-Org_{auto}) and after the image conversion (LDCT-$CONV_{auto}$). Manual scoring was performed on the CSCT images ($CSCT_{manual}$) and used as a reference standard. The accuracy of automated Agaston scores and risk severity categorization based on the automated scoring on LDCT scans was analyzed compared to the reference standard, using the Bland–Altman analysis, concordance correlation coefficient (CCC), and weighted kappa (κ) statistic.

Results: LDCT-$CONV_{auto}$ demonstrated a reduced bias for Agaston score, compared with $CSCT_{manual}$, than LDCT-Org_{auto} did (-3.45 vs. 206.7). LDCT-$CONV_{auto}$ showed a higher CCC than LDCT-Org_{auto} did (0.881 [95% confidence interval {CI}, 0.750–0.960] vs. 0.269 [95% CI, 0.129–0.430]). In terms of risk category assignment, LDCT-Org_{auto} exhibited poor agreement with $CSCT_{manual}$

Received: September 7, 2024 **Revised:** April 6, 2025 **Accepted:** April 21, 2025
Corresponding author: Young Joo Suh, MD, PhD, Department of Radiology, Severance Hospital, Research Institute of Radiological Science, Yonsei University College of Medicine, 50-1 Yonsei-ro, Seodaemun-gu, Seoul 03722, Republic of Korea
• E-mail: rongzusuh@gmail.com

(weighted κ = 0.115 [95% CI, 0.082–0.154]), whereas LDCT-CONV$_{auto}$ achieved good agreement (weighted κ = 0.792 [95% CI, 0.731–0.847]).
Conclusion: Deep learning-based conversion of LDCT images originally obtained with thin slices and a sharp kernel can enhance the accuracy of automated coronary artery calcium score measurement using the images.
Keywords: Calcium; Coronary vessels; Tomography, X-ray computed; Thorax; Artificial intelligence

INTRODUCTION

The coronary artery calcium (CAC) score derived from electrocardiogram (ECG)-gated computed tomography (CT) is a well-established marker for risk stratification of future cardiovascular events, offering incremental value beyond conventional risk factors [1-3]. The increasing use of chest CT scans and the advent of CT lung cancer screening have heightened interest in the incidental findings of CAC on non-ECG-gated chest CT scans [4]. The presence and severity of CAC detected on these scans can serve as prognostic markers for future cardiovascular outcomes across various populations [5-13]. Consequently, the assessment of CAC on non-ECG-gated chest CT scans has gained recognition. Acknowledging this, the 2016 guidelines of the Society of Cardiovascular Computed Tomography/Society of Thoracic Radiology recommend evaluating and reporting CAC on all non-contrast chest CT scans in patients aged ≥40 years [14]. Furthermore, the importance of reporting CAC as a significant incidental finding on low-dose chest CT (LDCT) performed for lung cancer screening is emphasized [15].

However, incidental CAC findings on non-ECG-gated CT scans are often underreported despite their clinical significance, primarily because these scans are typically performed for purposes other than cardiac evaluation. Additionally, performing manual Agatston scoring on LDCT scans is a skill-intensive task that demands additional processing time and dedicated software [14,16]. The use of automatic scoring methods for performing CAC assessment on LDCT scans could enhance reporting rates and broaden the utilization of this information. Several deep learning (DL)-based automated CAC scoring techniques developed for ECG-gated calcium scoring CT (CSCT) [17-21] have also been validated for use on LDCT scans, demonstrating generally favorable performance, albeit with variability across institutions that are largely attributable to differences in the scanning protocols employed [22,23]. This variability can contribute to inconsistencies in the performance of automatic software on LDCT scans [23]. Recently, DL-based image conversion techniques, such as adjusting slice thickness [24] or modifying the reconstruction kernel [25,26], have been applied to chest CT to improve reproducibility in quantifying emphysema or radiomic features of thoracic lesions. Implementation of these image conversion techniques is expected to mitigate the effects of variability in LDCT scanning protocols. Therefore, we hypothesized that the application of DL-based image conversion techniques would enhance the performance of automated CAC quantification on LDCT images reconstructed with thin slicethickness and a sharp kernel.

This study aimed to evaluate the impact of image conversion on the accuracy of automated CAC quantification using 1-mm or 1.25-mm, sharp-kernel, non-gated LDCT images collected from multiple institutions.

MATERIALS AND METHODS

This study was approved by the Institutional Review Boards of the participating hospitals (IRB Nos. KC22RIDI0156, 2021-12-027, 2022GR0064, 2021AS0371, 2022-01-001, 2021-0303, 2021-12-029, and 4-2021-1589). The requirement for informed consent was waived due to the retrospective design of the study.

Participants

In this study, we conducted a post-hoc analysis using data from a large retrospective cohort to evaluate the reliability of CAC scoring on LDCT scans. The original cohort comprised participants who met the eligibility criteria and were retrospectively enrolled from eight participating academic hospitals (Fig. 1). The inclusion criteria were as follows: 1) being an adult (age ≥18 years) and having undergone both non-ECG-gated LDCT and ECG-gated CSCT within a 6-month interval between January 2010 and December 2020 and 2) acquisition of CT scans using a scanner with 64 or more detector rows. A total of 1569 participants met these inclusion criteria. The exclusion criteria were as follows: 1) having previously undergone coronary stent insertion or coronary bypass graft surgery before the CT scan (n = 12), 2) inadequate LDCT image

https://doi.org/10.3348/kjr.2025.0177

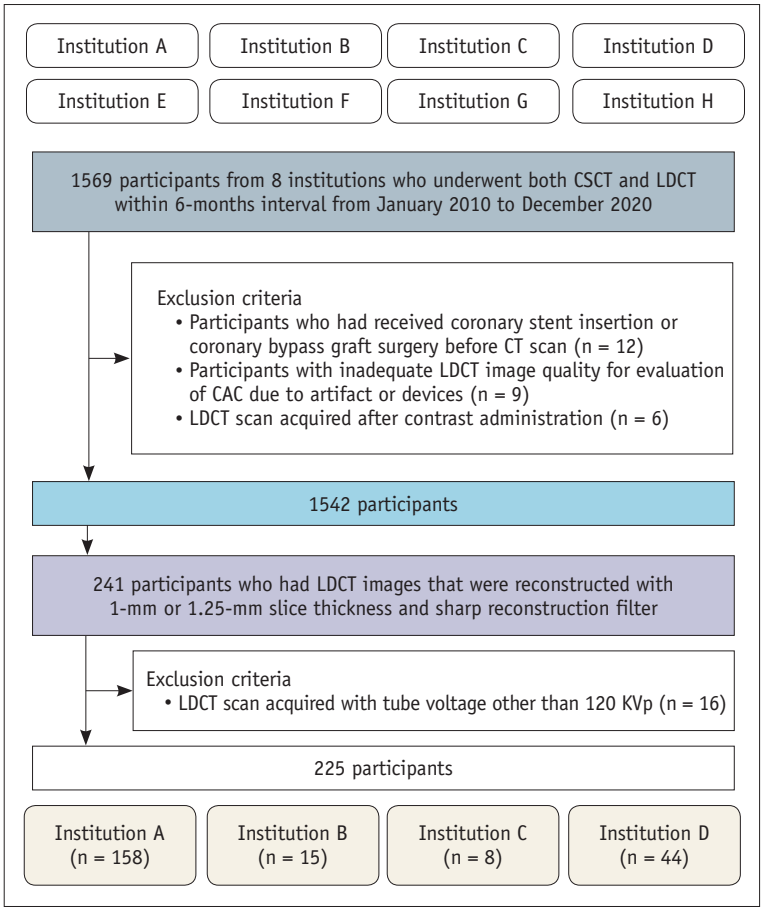

Fig. 1. Participant flowchart. CSCT = calcium scoring computed tomography, LDCT = low-dose computed tomography, CAC = coronary artery calcium

quality for CAC evaluation due to artifacts or the presence of devices (n = 9), and 3) acquisition of LDCT scans after contrast administration (n = 6). Ultimately, 1542 CSCT and 1542 LDCT scans were used for CAC scoring. From these, we selected the CT scans of 241 participants whose LDCT images were reconstructed with a slice thickness of 1-mm or 1.25-mm and a sharp kernel. Additionally, we excluded 16 participants whose LDCT scans were acquired using a tube voltage other than 120 kV, considering that the standard protocol for CSCT scanning uses 120 kV and that various tube voltage settings in LDCT can affect CAC. Finally, 225 participants were included in this study.

CT Datasets: Image Acquisition and Reconstruction

The detailed CT image acquisition and reconstruction protocols are summarized in Supplementary Table 1. All CSCT scans were reconstructed with a standard kernel and a slice thickness of 2.5-mm or 3-mm. Non-ECG-gated LDCT scans were reconstructed with a slice thickness of 1-mm or 1.25-mm and a sharp reconstruction filter (kernel).

Image Conversion

For LDCT, image conversion was performed to simulate conventional CSCT using a proprietary software program (AVIEW CAC, version 1.1.43; Coreline Soft, Co., Ltd., Seoul, South Korea), which incorporated two algorithms: 1) DL-based kernel conversion (KC) algorithm, which generates CT images simulating standard-dose, low-frequency kernels from low-dose, high-frequency kernels [27,28]. It enables direct transformations on reconstructed images without the need for sinogram data. KC was performed using a weighting of 0.5. 2) Thickness conversion (TC), which constructs volume data using the raysum method, employing an average value for each ray for the desired plane in volume rendering. TC was performed to convert images with a thickness of 1-mm or 1.25-mm to 3-mm. Four sets of LDCT images were used for analysis (Fig. 2): original images without conversion (LDCT-Org), images with KC only (LDCT-KC), images with TC only (LDCT-TC), and images with both KC and TC (LDCT-CONV). Image noise was measured on four LDCT datasets and was defined as the standard deviation (SD)

 https://doi.org/10.3348/kjr.2025.0177

of the measured Hounsfield units (HU) within the circular region of interests in the ascending aorta on the slice image at the level of the left main coronary artery.

Automated CAC Scoring

Automated CAC scoring was performed on four image datasets of LDCT scans for each participant using a commercial software (AVIEW CAC, Coreline Soft, Co. Ltd.). The software was developed using the concept of an atlas-based automated CAC scoring system empowered by DL technology [21] and has been validated for automated CAC scoring in both CSCT and LDCT in previous studies [22,23,29,30]. For each CT scan, the Agatston score, CAC volume score (mm^3), and peak CAC density were calculated at the per-artery level for the four main coronary arteries and at the per-subject level.

Reference CAC Scoring

Manual CAC scoring was performed on CSCT scans ($CSCT_{manual}$) and used as a reference standard. Manual scoring was performed independently by two board-certified expert radiologists, each with 10 and 11 years of experience in cardiothoracic imaging, using commercial software (AVIEW CAC, Coreline Soft, Co. Ltd.), without the assistance of an automatic algorithm. Following thresholding (>130 HU) with a colored overlay, the CACs were manually labeled by the readers according to their anatomical location (i.e., left main, left anterior descending [LAD], left circumflex, and right coronary arteries). The manual scoring results of the two radiologists were extracted, and the Agatston score,

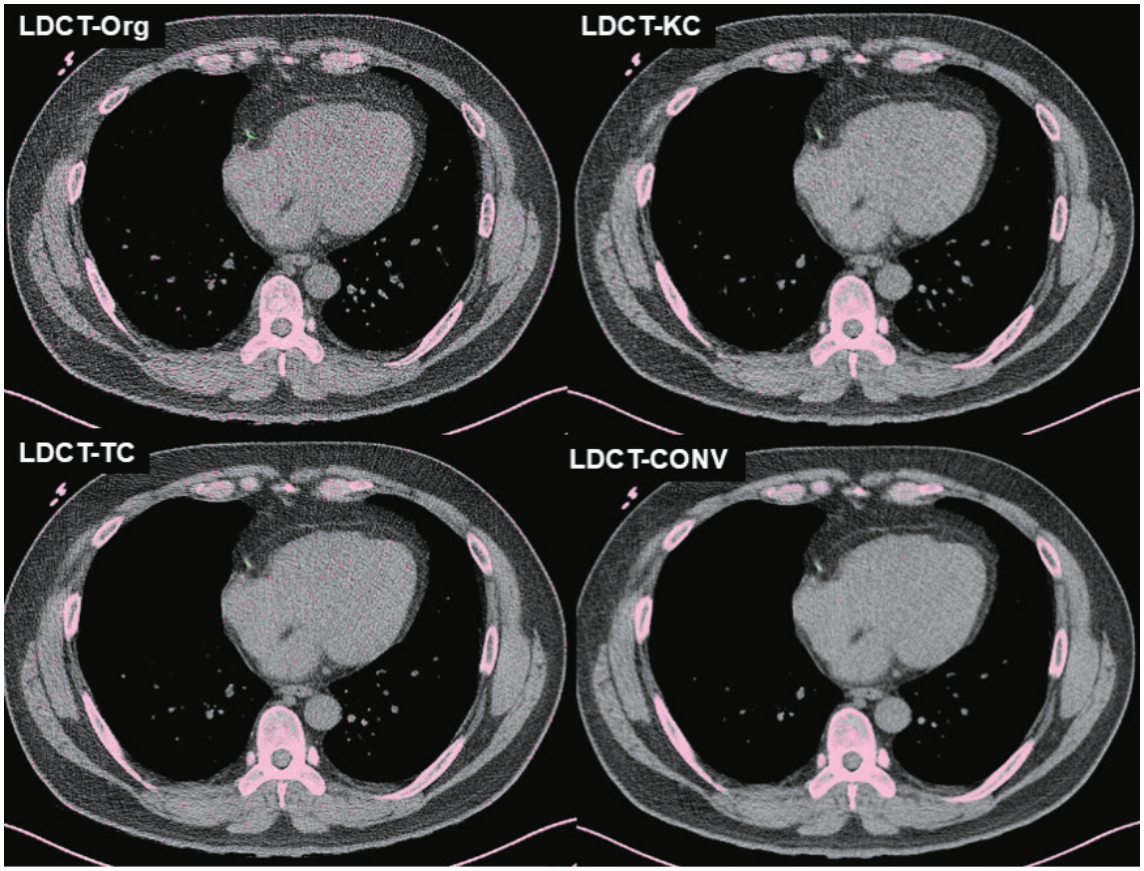

Fig. 2. Examples of image conversion. Original image without conversion (LDCT-Org), image with kernel conversion only (LDCT-KC), image with slice thickness conversion only (LDCT-TC), and image with both kernel and slice thickness conversion (LDCT-CONV). The Agaston scores of the reference standard ($CSCT_{manual}$), $LDCT\text{-}Org_{auto}$, $LDCT\text{-}KC_{auto}$, $LDCT\text{-}TC_{auto}$, and $LDCT\text{-}CONV_{auto}$ were 56, 106, 64, 67, and 58, respectively. LDCT = low-dose chest computed tomography, LDCT-Org = original image without conversion, LDCT-KC = LDCT image with kernel conversion only, LDCT-TC = LDCT image with slice thickness conversion only, LDCT-CONV = LDCT image with both kernel and slice thickness conversion, CSCT = calcium scoring computed tomography, $CSCT_{manual}$ = manual scoring on calcium scoring CT, $LDCT\text{-}Org_{auto}$ = automatic scoring on original LDCT images without conversion, $LDCT\text{-}KC_{auto}$ = automatic scoring on LDCT images with kernel conversion, $LDCT\text{-}TC_{auto}$ = automatic scoring on original LDCT images with slice thickness conversion, $LDCT\text{-}CONV_{auto}$ = automatic scoring on LDCT images with both kernel and slice thickness conversion

https://doi.org/10.3348/kjr.2025.0177

Korean Journal of Radiology
KJR

volume score, and number of CAC lesions were compared at the per-subject and per-artery levels. When the two radiologists' results differed, a consensus reading session was conducted to resolve the disagreement in CAC scoring results. The results obtained through the consensus reading sessions were used to establish the reference standard.

Statistical Analyses

The results of the image noise analysis of the four LDCT datasets were compared using repeated-measures analysis of variance.

The accuracies of the quantitative CAC parameters (Agatston score, volume score, and peak density) and risk categorization according to the automated Agatston score on the four LDCT datasets were assessed by comparing them to the $CSCT_{manual}$ as the reference standard. To analyze the accuracy of the quantitative parameters, Bland–Altman analysis was employed to determine the bias, and 95% limits of agreement and Lin's concordance correlation coefficient (CCC) were employed. CCC was interpreted as follows: values >0.90, 0.80–0.90, 0.65–0.80, and <0.65 indicate excellent, substantial, moderate, and poor agreement, respectively [31]. To analyze the accuracy of cardiovascular risk stratification using the automated Agatston score, CAC severity was categorized into the following groups based on the Mayo criteria [32]: 0, 1–10, 11–100, 101–400, and >400. The agreement of CAC severity categories between automated scoring on LDCT-Org (LDCT-Org_{auto}) and that on LDCT-CONV (LDCT-$CONV_{auto}$) with $CSCT_{manual}$ was assessed using the Cohen linearly weighted kappa (κ) statistic. In cases of disagreement in the risk category between $CSCT_{manual}$ and LDCT-$CONV_{auto}$, we determined the underlying reasons for this disagreement. In addition to the analysis including all participants, a subgroup analysis was performed including participants with CAC >0 on $CSCT_{manual}$.

Bonferroni-adjusted post-hoc *P*-values <0.0083 were considered as indicative of a statistically significant difference for multiple comparisons of image noise between the four LDCT datasets. Otherwise, a *P*-value <0.05 was considered as indicative of a statistically significant difference.

RESULTS

Participants

The baseline clinical characteristics and CT imaging

Table 1. Baseline characteristics of the participants in the study cohorts

	All (n = 225)	Institution A (n = 158)	Institution B (n = 15)	Institution C (n = 8)	Institution D (n = 44)
Sex, male	163 (72.4)	110 (69.6)	12 (80.0)	5 (62.5)	36 (81.8)
Age, yrs	57.3 ± 9.2	58.0 ± 8.6	57.71 ± 6.8	57.4 ± 13.8	54.6 ± 10.7
Body mass index, kg/m^2	24.3 ± 3.4	24.7 ± 3.7	24.5 ± 3.0	24.8 ± 2.1	25.0 ± 2.8
Heart rate, beats/min	58.3 ± 8.6	56.8 ± 7.5	66.2 ± 9.3	71 ± 10.1	N/A
Hypertension	75 (33.3)	61 (38.6)	3 (20.0)	2 (25.0)	9 (20.5)
Diabetes mellitus	31 (13.8)	22 (13.9)	1 (6.7)	3 (37.5)	5 (11.4)
Smoking					
Current smoker	62 (27.6)	46 (29.1)	2 (13.3)	3 (37.5)	11 (25.0)
Ex-smoker	55 (24.4)	38 (24.1)	1 (6.7)	0 (0)	16 (36.4)
Dyslipidemia	48 (21.3)	37 (23.4)	5 (33.3)	2 (25.0)	4 (9.1)
Indication of LDCT					
Screening	180 (80.0)	115 (72.8)	14 (93.3)	7 (87.5)	44 (100)
Symptomatic or other clinical purpose	45 (20.0)	43 (27.2)	1 (6.7)	1 (12.5)	0 (0)
Agatston score on $CSCT_{manual}$	0 (0–28.9)	0 (0–43.7)	110.2 (0–23.2)	0 (0–14.3)	0 (0–4.0)
Agatston score-based risk category in $CSCT_{manual}$					
0	132 (58.7)	90 (57.0)	7 (46.7)	5 (62.5)	30 (68.2)
1–10	16 (7.1)	11 (7.0)	1 (6.7)	0 (0)	4 (9.1)
11–100	48 (21.3)	31 (19.6)	7 (46.7)	2 (25.0)	8 (18.2)
101–400	18 (8.0)	17 (10.8)	0 (0)	0 (0)	1 (2.3)
>400	11 (4.9)	9 (5.7)	0 (0)	1 (12.5)	1 (2.3)

Data are presented as the number of patients (%), mean ± standard deviation, or median (interquartile range).
N/A = not available, LDCT = low-dose computed tomography, $CSCT_{manual}$ = manual scoring on calcium scoring computed tomography

https://doi.org/10.3348/kjr.2025.0177

Table 2. Accuracy of automated Agatston score, CAC volume, and peak density on LDCT-Org_{auto}, LDCT-KC_{auto}, LDCT-TC_{auto}, and LDCT-$CONV_{auto}$ in all participants (n = 225)

	Agaston score				Volume score				Peak density			
	LDCT-Org_{auto}	LDCT-KC_{auto}	LDCT-TC_{auto}	LDCT-$CONV_{auto}$	LDCT-Org_{auto}	LDCT-KC_{auto}	LDCT-TC_{auto}	LDCT-$CONV_{auto}$	LDCT-Org_{auto}	LDCT-KC_{auto}	LDCT-TC_{auto}	LDCT-$CONV_{auto}$
Total												
Mean bias	206.7	36.22	37.63	-3.45	210.77	39	36.83	-3.61	551.27	241.08	185.75	6.48
B-A	-389.15	-143.65	-212.48	-147.01	-334.90	-123.18	-181.42	-119.52	-98.48	-87.28	-167.88	-252.03
95% LOA	−802.54	−216.09	−287.74	−140.10	−756.45	−201.18	−255.08	−112.30	−1201.01	−569.43	−539.37	−264.99
CCC	0.269	0.851	0.710	0.881	0.212	0.818	0.675	0.883	0.388	0.681	0.737	0.891
(95% CI)	(0.129, 0.430)	(0.767, 0.906)	(0.549, 0.848)	(0.750, 0.960)	(0.100, 0.350)	(0.720, 0.883)	(0.515, 0.821)	(0.748, 0.964)	(0.341, 0.436)	(0.628, 0.734)	(0.687, 0.780)	(0.854, 0.919)
LM												
Mean bias	14.97	3.02	2.85	-1	15.27	3.09	2.69	-0.76	359.64	125.87	90.37	1.81
B-A	-44.18	-27.18	-40.98	-34.07	-37.32	-22.09	-33.95	-27.41	-225.26	-245.52	-226.67	-229.71
95% LOA	−74.12	−33.23	−46.69	−32.06	−67.85	−28.27	−39.33	−25.89	−944.53	−497.26	−407.41	−233.33
CCC	0.502	0.842	0.704	0.785	0.441	0.834	0.684	0.795	0.333	0.613	0.686	0.775
(95% CI)	(0.301, 0.670)	(0.729, 0.921)	(0.555, 0.836)	(0.598, 0.908)	(0.253, 0.606)	(0.714, 0.916)	(0.526, 0.817)	(0.631, 0.908)	(0.243, 0.427)	(0.501, 0.716)	(0.577, 0.767)	(0.663, 0.865)
LAD												
Mean bias	56.59	12.82	11.37	1.48	55.48	12.05	9.88	0.39	457.26	180.28	130.98	-5.01
B-A	-147.01	-69.58	-84.54	-60.75	-125.99	-52.98	-67.56	-45.21	-214.96	-195.26	-267.83	-208.47
95% LOA	−260.19	−95.21	−107.28	−63.72	−236.94	−77.08	−87.32	−45.98	−1129.48	−555.82	−529.80	−198.45
CCC	0.456	0.878	0.809	0.921	0.382	0.872	0.798	0.929	0.375	0.689	0.715	0.914
(95% CI)	(0.208, 0.681)	(0.763, 0.937)	(0.590, 0.925)	(0.820, 0.971)	(0.158, 0.607)	(0.758, 0.933)	(0.586, 0.921)	(0.819, 0.981)	(0.319, 0.429)	(0.630, 0.747)	(0.642, 0.777)	(0.878, 0.943)
LCX												
Mean bias	46.27	9.15	9.88	-0.43	48.42	10.47	9.68	0.01	370.95	151.11	91.51	3.78
B-A	-121.34	-63.30	-80.90	-67.75	-107.96	-54.88	-69.84	-56.64	-3.29	-129.54	-187.79	-192.68
95% LOA	−213.87	−81.59	−100.66	−66.90	−204.79	−75.82	−89.20	−56.66	−745.19	−431.75	−370.81	−200.24
CCC	0.339	0.763	0.656	0.733	0.287	0.739	0.631	0.742	0.298	0.588	0.690	0.820
(95% CI)	(0.129, 0.514)	(0.636, 0.853)	(0.431, 0.818)	(0.364, 0.971)	(0.104, 0.458)	(0.617, 0.817)	(0.412, 0.796)	(0.400, 0.964)	(0.183, 0.420)	(0.430, 0.721)	(0.541, 0.806)	(0.714, 0.892)
RCA												
Mean bias	88.94	11.27	13.52	-3.49	91.55	13.4	14.56	-3.29	420.13	175.05	134.85	4.81
B-A	-167.68	-54.23	-92.83	-58.59	-145.78	-51.77	-81.17	-51.57	30.64	-124.31	-178.82	-236.99
95% LOA	−345.56	−76.76	−119.88	−51.61	−328.88	−78.57	−110.29	−44.99	−809.62	−474.42	−448.53	−246.62
CCC	0.124	0.796	0.527	0.815	0.097	0.732	0.489	0.807	0.294	0.547	0.586	0.757
(95% CI)	(0.055, 0.200)	(0.656, 0.895)	(0.376, 0.695)	(0.717, 0.869)	(0.040, 0.164)	(0.539, 0.852)	(0.353, 0.642)	(0.707, 0.870)	(0.216, 0.372)	(0.453, 0.634)	(0.472, 0.685)	(0.668, 0.825)

CAC = coronary artery calcium, LDCT = low-dose computed tomography, LDCT-Org_{auto} = automatic scoring on original LDCT images without conversion, LDCT-KC_{auto} = automatic scoring on LDCT images with kernel conversion, LDCT-TC_{auto} = automatic scoring on original LDCT images with slice thickness conversion, LDCT-$CONV_{auto}$ = automatic scoring on LDCT images with both kernel and slice thickness conversion, B-A = Bland-Altman, LOA = limits of agreement, CCC = concordance correlation coefficient, CI = confidence interval, LM = left main artery, LAD = left anterior descending artery, LCX = left circumflex artery, RCA = right coronary artery

Korean Journal of Radiology
KJR

parameters are presented in Table 1 and Supplementary Table 1. Six types of CT machines from two companies were used for acquiring CSCT scans, and eight types of CT machines from three companies were used for obtaining LDCT scans. The CSCT and LDCT scans were acquired using machines from the same companies in 222 participants (98.7%) and using the same type of machine in 184 participants (81.8%). The median Agatston score was 0 (interquartile range [IQR], 0 to 28.9) on $CSCT_{manual}$.

Comparison of Image Noise Among the Four LDCT Datasets

The median image noise was significantly different between the four LDCT datasets, showing the highest values in LDCT-Org (104.9 HU, IQR 90.1 to 125.1 HU) and decreasing in the order of LDCT-TC (67.0 HU, IQR 57.8 to 83.1 HU), LDCT-KC (59.6 HU, IQR 51.3 to 73.4 HU), and LDCT-CONV (38.2 HU, IQR 33.3 to 48.0 HU) (uncorrected $P < 0.0083$, indicating statistical significance for multiple comparisons).

Accuracy of Automatic Quantitative CAC Parameters on LDCT Before and After Image Conversion

The Bland–Altman analysis and CCCs for automatic CAC parameters on the four LDCT image datasets compared with $CSCT_{manual}$ are shown in Table 2 and Figure 3. The mean biases with the SD of the Agatston scores on $LDCT\text{-}Org_{auto}$, $LDCT\text{-}KC_{auto}$, $LDCT\text{-}TC_{auto}$, and $LDCT\text{-}CONV_{auto}$, compared with $CSCT_{manual}$, were 206.7, 36.22, 37.63, and -3.45, respectively. The CCCs for the Agatston score, volume score, and peak density were highest between $CSCT_{manual}$ and $LDCT\text{-}CONV_{auto}$ (0.881 [95% CI 0.750–0.960], 0.883 [95% CI 0.748–0.964], and 0.891 [95% CI 0.854–0.919], respectively), whereas they were lowest between $CSCT_{manual}$ and $LDCT\text{-}Org_{auto}$ (0.269 [95% CI 0.129–0.430], 0.212 [95% CI 0.100–0.350], and 0.388 [95% CI 0.341–0.436], respectively). The accuracies of the volume score and peak density were highest for $LDCT\text{-}CONV_{auto}$ and lowest for $LDCT\text{-}Org_{auto}$. The per-artery analysis showed a tendency similar to that of the per-subject analysis in terms of the Agatston score, volume score, and peak density. However, in all images processed using DL-based image conversion, the CCC values for the Agatston score, volume score, and peak density were higher in the LAD than in the other vessels. Notably, in the case of $LDCT\text{-}CONV_{auto}$, the CCC values for the Agatston score, volume score, and peak density demonstrated excellent reliability only in the LAD, whereas the other vessels showed moderate to substantial reliability.

Accuracy of Risk Category Assignment Using Automatic Agaston Scoring on LDCT Before and After Image Conversion

Table 3 presents the kappa coefficients comparing both $LDCT\text{-}Org_{auto}$ and $LDCT\text{-}CONV_{auto}$ with $CSCT_{manual}$. Figure 4 and Supplementary Figure 1 present confusion matrices comparing the automatic scoring on the four LDCT image datasets with $CSCT_{manual}$. $LDCT\text{-}Org_{auto}$ demonstrated poor agreement with $CSCT_{manual}$, with a weighted κ value of 0.115 (95% CI 0.082–0.154). In contrast, $LDCT\text{-}CONV_{auto}$ achieved good agreement with $CSCT_{manual}$, showing a weighted κ value of 0.792 (95% CI 0.731–0.847).

$LDCT\text{-}CONV_{auto}$ correctly assigned 77.3% (174/225) to the same risk category as $CSCT_{manual}$, 19.1% (43/225) were placed in a neighboring category, and 3.6% (8/225) differed by two categories from $CSCT_{manual}$. Among the 51 (22.7%)

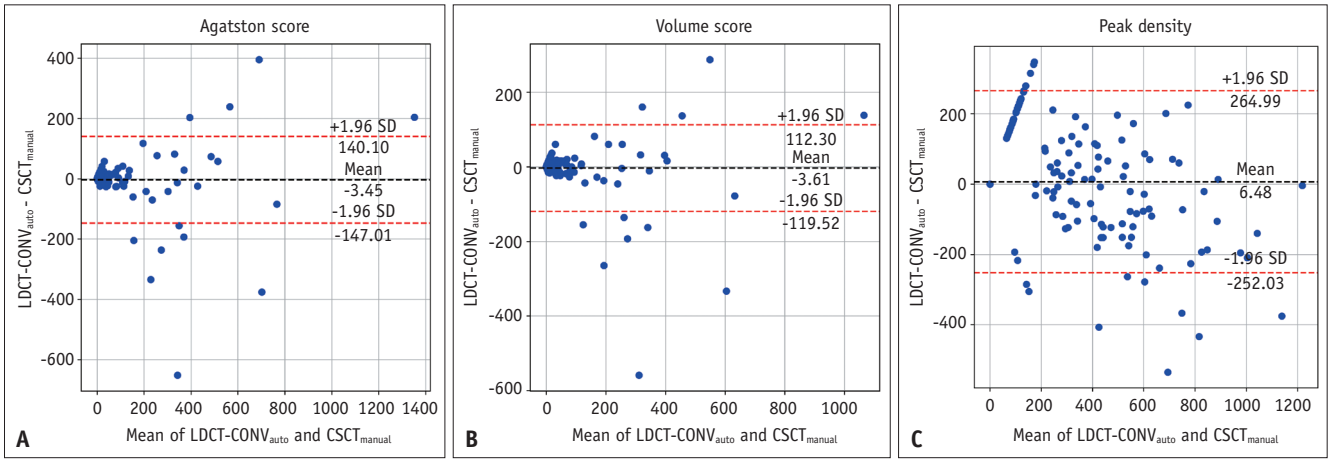

Fig. 3. Bland–Altman plots for the **(A)** Agatston score, **(B)** volume score, and **(C)** peak density on $LDCT\text{-}CONV_{auto}$ compared with $CSCT_{manual}$ in all participants (n = 225). LDCT = low-dose computed tomography, $LDCT\text{-}CONV_{auto}$ = automatic scoring on LDCT images with both kernel and slice thickness conversion, $CSCT_{manual}$ = manual scoring on calcium scoring computed tomography, SD = standard deviation

https://doi.org/10.3348/kjr.2025.0177

participants showing one or more category differences, the risk categories of 37 (16.4%) were overestimated and 14 (6.2%) were underestimated. Overestimations primarily occurred because of noise near the coronary artery areas being misinterpreted as CAC (23/37, 62.2%), pulmonary veins adjacent to the heart being mistaken for left circumflex artery calcification (8/37, 21.6%), and motion artifacts (4/37, 10.8%) (Supplementary Figs. 2, 3). In two cases of overestimation (5.4%), calcifications that were not visible on CSCT scans were detected on LDCT scans (Supplementary Fig. 3). All 14 cases of underestimation occurred entirely due to detection failure, which resulted from the reduction of calcification to <130 HU during the image reconstruction process (Supplementary Fig. 4).

Table 3. Agreement in risk category assignment using Agaston scoring between LDCT and $CSCT_{manual}$ in all participants (n = 225)

Index	Weighted kappa (95% CI)
$LDCT\text{-}Org_{auto}$	0.115 (0.082, 0.154)
$LDCT\text{-}KC_{auto}$	0.424 (0.360, 0.492)
$LDCT\text{-}TC_{auto}$	0.442 (0.375, 0.510)
$LDCT\text{-}CONV_{auto}$	0.792 (0.731, 0.847)

LDCT = low-dose computed tomography, $CSCT_{manual}$ = manual scoring on calcium scoring computed tomography, CI = confidence interval, $LDCT\text{-}Org_{auto}$ = automatic scoring on original LDCT images without conversion, $LDCT\text{-}KC_{auto}$ = automatic scoring on LDCT images with kernel conversion, $LDCT\text{-}TC_{auto}$ = automatic scoring on original LDCT images with slice thickness conversion, $LDCT\text{-}CONV_{auto}$ = automatic scoring on LDCT images with both kernel and slice thickness conversion

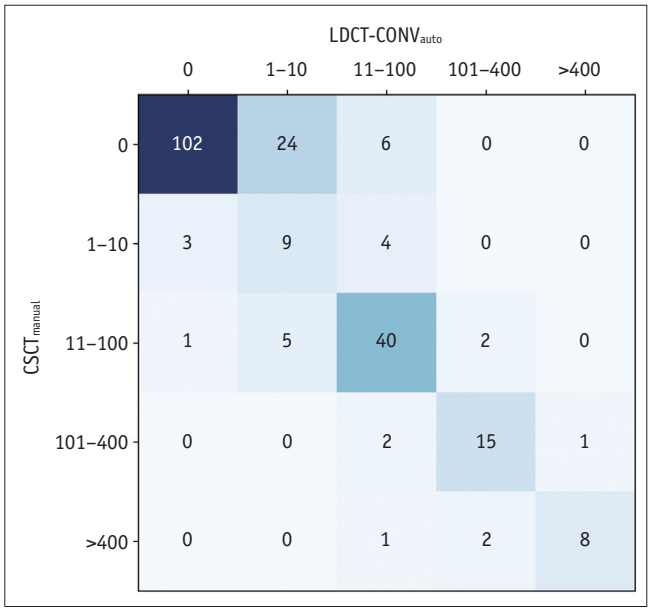

Fig. 4. Confusion matrices of $LDCT\text{-}CONV_{auto}$ with $CSCT_{manual}$ for risk category assignment. $LDCT\text{-}CONV_{auto}$ = automatic scoring on LDCT images with both kernel and slice thickness conversion, $CSCT_{manual}$ = manual scoring on calcium scoring computed tomography

Subgroup Analysis

In the subgroup of participants with CAC > 0 (n = 93) according to $CSCT_{manual}$, the mean biases for the Agatston score on $LDCT\text{-}Org_{auto}$, $LDCT\text{-}KC_{auto}$, $LDCT\text{-}TC_{auto}$, and $LDCT\text{-}CONV_{auto}$, compared with $CSCT_{manual}$, were 261.96, 65.98, 56.23, and -10.65, respectively (Supplementary Table 2). $LDCT\text{-}Org_{auto}$ exhibited the lowest CCC, indicating poor reliability (0.281 [95% CI, 0.084–0.496]) of the Agatston score in the per-subject analysis. In contrast, $LDCT\text{-}KC_{auto}$ and $LDCT\text{-}TC_{auto}$ showed moderate to substantial reliability (CCC 0.823 [95% CI, 0.712–0.891] and 0.664 [95% CI, 0.441–0.831], respectively). $LDCT\text{-}CONV_{auto}$ demonstrated the highest CCC (0.855 [95% CI, 0.700–0.951]) among the datasets, indicating excellent reliability. For risk category assignment, $LDCT\text{-}Org_{auto}$ demonstrated poor agreement with $CSCT_{manual}$, with a weighted κ value of 0.194 (95% CI, 0.103–0.292, Supplementary Table 3). In contrast, $LDCT\text{-}CONV_{auto}$ achieved good agreement with $CSCT_{manual}$, showing a weighted κ value of 0.740 (95% CI, 0.624–0.836).

DISCUSSION

The present study demonstrated the effect of combined KC and TC techniques on fully automated CAC scoring in non-gated LDCT scans with thin slices and sharp kernel reconstruction. The image conversion performed for LDCT images significantly decreased image noise and improved the agreement and reliability of automatic CAC scoring, compared with $CSCT_{manual}$, at both per-subject and per-artery levels.

LDCT is usually reconstructed with thin slice thickness and a sharp kernel to achieve a higher spatial resolution, which is beneficial for imaging high-contrast structures, such as bones or lungs [33,34]. However, this setting increases image noise and compromises the evaluation of low-contrast structures, such as the mediastinum or soft tissue, hindering accurate CAC measurement on LDCT scans [23]. Previous studies indicated that reconstruction of LDCT scans with a smooth kernel, as opposed to a sharp kernel, is more reliable method for evaluating CAC [35]. Additionally, thinner slices significantly increase the CAC scores [22,36]. Moreover, the performance of the automatic CAC scoring software, in addition to the CAC score itself, could potentially be influenced by the LDCT scanning protocol. Although several

https://doi.org/10.3348/kjr.2025.0177

Korean Journal of Radiology
KJR

studies have shown the clinical utility of DL-based automatic CAC measurement in LDCT, such as the correlation between DL-based CAC on CSCT and LDCT scans [22,37-39], or its prognostic value [40], the LDCT scans in these studies were typically reconstructed with smooth/soft tissue kernels or thicker slices. Indeed, a recent multi-center study found that the imaging protocols of LDCT datasets varied across participating institutions, leading to performance differences in automatic software for CAC measurement based on the reconstruction kernel or slice thickness used [23]. We hypothesized that image conversion, including the conversion of kernel and slice thickness in LDCT scans, could facilitate a more accurate evaluation of CAC.

Our image conversion technique may offer a potential solution for minimizing the influence of variations among LDCT protocols. Using DL-based image conversion, we effectively reduced image noise, which likely contributed to the improved accuracy of automated CAC scoring. Consequently, the Agatston score, volume score, and peak density demonstrated excellent agreement with the reference standard for the multi-center datasets acquired using CT scanners from various manufacturers. These findings demonstrate the potential clinical utility of automated CAC scoring on converted LDCT images. This approach is a potential practical solution for achieving faster and more efficient CAC evaluation in clinical practice.

In addition to image conversion, performing additional image reconstruction of LDCT scans using the same parameters as CSCT (e.g., 2.5-mm or 3-mm slice thickness and soft kernel) could also be considered a solution. However, this approach has limitations, as previous studies have indicated that the CAC evaluation accuracy may decrease when LDCT images are acquired at slice thicknesses ≥2.5 mm. One study demonstrated higher agreement with CSCT for CAC severity classification with automated measurement at a slice thickness of 1-mm ($\kappa > 0.8$) compared with 2.5-mm slice thickness ($\kappa = 0.776$) [22]. Similarly, another study reported that CAC measurement on LDCT scans with 2.5-mm slice thickness tended to be underestimated, with 12.8% of high-risk CAC scores underestimated, compared with ECG-gated CT with 2.5-mm slice thickness [41]. Although these studies did not thoroughly examine variations in other CT parameters or among CT vendors, the findings suggest that LDCT with thinner slice thickness may offer a more accurate CAC assessment than does LDCT with 2.5-mm or 3-mm slice thickness. In fact, two cases of CAC overestimation on LDCT-$CONV_{auto}$ in our study were due to the identification of small calcifications that were undetected on CSCT. Practical considerations, such as data storage capacity, radiologist workload and preferences, when reviewing multiple image series, and institutional differences in clinical practice should also be considered before performing additional image reconstructions. Therefore, further well-designed research is necessary to compare the accuracy between automated CAC measurement on converted LDCT images that were originally reconstructed with thin slices and sharp kernel and those reconstructed with 2.5-mm or 3-mm slices and soft kernel.

Despite the implementation of image conversion in our study, several unresolved issues concerning automated CAC measurement on LDCT remain, necessitating further investigation. First, in addition to the impact of high image noise, motion artifacts caused by the absence of ECG-gating contribute to inaccurate CAC scoring and the misclassification of risk categories. In our study, 10.8% (4/37) of the overestimations of CAC severity categories on LDCT-$CONV_{auto}$ were due to motion artifacts. These are challenging to overcome due to the inherent characteristics of non-ECG-gated chest CT. Second, 72.0% of cases in our study used iterative reconstruction (IR) on LDCT scans. Previous studies have reported that IR tends to yield lower CAC scores, compared with filtered back projection [42-44]; however, IR does not significantly affect CAC severity classification. Given that LDCT scans without IR have high image noise and reduced image quality, omitting IR or performing additional filtered back projection for CAC measurement on LDCT scans may not be practical from the standpoint of resources and reader workload. Nonetheless, as this study was not specifically designed to evaluate the influence of IR on CAC scoring, further research is needed to explicitly address this issue. Finally, the most common cause of CAC score underestimation on LDCT scans was the attenuation values of calcifications being <130 HU as a result of image conversion. The 130-HU threshold currently remains critical for CAC measurement in clinical practice; thus, future studies should either consider adjusting this threshold or develop an optimized method for weighting KC.

Our study has some limitations. First, our datasets consisted of a high percentage of participants with CAC = 0 in the reference standard and CT scans acquired using scanners from a specific manufacturer, which could have overestimated the impact of image conversion or limited the capacity to generalize the findings to a broader spectrum of scanner models. Although LDCT-$CONV_{auto}$ demonstrated good

 https://doi.org/10.3348/kjr.2025.0177

performance in our subgroup analysis of participants with CAC >0, further studies using a large number of participants with positive CAC or CT scans with varying protocols and equipment are required to establish the broader applicability of DL-based image conversion. Second, we included participants who underwent CSCT and LDCT within a 6-month interval. Although performing two CT scans on the same day would be optimal to minimize the impact of potential CAC progression, we set the scan interval based on the results of previous studies. A previous study utilizing data from the Multi-Ethnic Study of Atherosclerosis found that the annual incidence rate of CAC in Asian individuals (Chinese) free of CAC at baseline was 4.7% among women and 4.4% among men [45]. Furthermore, among Chinese patients with detectable CAC at baseline, the median annual progression rate of CAC was observed to be 12.7 Agatston units per year. Additionally, previous studies comparing the CAC scores between CSCT and LDCT demonstrated a high correlation and accuracy for intervals up to a median of 7–10 months [46,47]. Therefore, a 6-month interval was deemed acceptable for maintaining consistency between the CAC scores obtained from CSCT and LDCT. Third, we did not correlate the cardiovascular outcomes of the participants with our results owing to the relatively small sample size. Additional multi-center studies are needed to validate the image conversion and correlate the findings with clinical prognosis.

In conclusion, automated CAC measurement using image conversion on LDCT scans originally obtained with thin slices and sharp kernel demonstrated excellent accuracy, compared with manual scoring, in multi-institutional datasets. However, further improvements in image conversion techniques are required to achieve more accurate results.

Supplement

The Supplement is available with this article at https://doi.org/10.3348/kjr.2025.0177.

Availability of Data and Material

The datasets generated or analyzed during the study are available from the corresponding author on reasonable request.

Conflicts of Interest

Dong Hyun Yang, a Section Editor of the *Korean Journal of Radiology*, was not involved in the editorial evaluation or decision to publish this article.

Sehyun Hong, is an employee of Coreline Soft, Co., Ltd., which provided the software and technical support.
The remaining authors have declared no conflicts of interest.

Author Contributions

Conceptualization: Cherry Kim, Young Joo Suh. Data curation: Cherry Kim, Won-Seok Yoo, Jin Young Kim, Suyon Chang, Chan Ho Park, Su Jin Hong, Dong Hyun Yang, Hwan Seok Yong, Young Joo Suh. Formal analysis: Cherry Kim, Sehyun Hong, Hangseok Choi, Won-Seok Yoo, Young Joo Suh. Funding acquisition: Young Joo Suh. Investigation: Cherry Kim, Young Joo Suh. Methodology: Cherry Kim, Sehyun Hong, Hangseok Choi, Jin Young Kim, Suyon Chang, Chan Ho Park, Su Jin Hong, Dong Hyun Yang, Hwan Seok Yong, Marly van Assen, Carlo N. De Cecco, Young Joo Suh. Project administration: Young Joo Suh. Resources: Cherry Kim, Young Joo Suh. Software: Cherry Kim, Young Joo Suh. Supervision: Cherry Kim, Young Joo Suh. Validation: Cherry Kim, Young Joo Suh. Visualization: Cherry Kim, Sehyun Hong, Young Joo Suh. Writing—original draft: Cherry Kim, Young Joo Suh. Writing—review & editing: all authors.

ORCID IDs

Cherry Kim
https://orcid.org/0000-0002-3361-5496
Sehyun Hong
https://orcid.org/0009-0000-2345-8688
Hangseok Choi
https://orcid.org/0000-0001-7412-8160
Won-Seok Yoo
https://orcid.org/0000-0002-3871-7133
Jin Young Kim
https://orcid.org/0000-0001-6714-8358
Suyon Chang
https://orcid.org/0000-0002-9221-8116
Chan Ho Park
https://orcid.org/0000-0002-0653-4666
Su Jin Hong
https://orcid.org/0000-0002-0634-4731
Dong Hyun Yang
https://orcid.org/0000-0001-5477-558X
Hwan Seok Yong
https://orcid.org/0000-0003-0247-8932
Marly van Assen
https://orcid.org/0000-0003-4044-4426
Carlo N. De Cecco
https://orcid.org/0000-0002-2956-3101

Young Joo Suh
https://orcid.org/0000-0002-2078-5832

Funding Statement

This research was supported by the Researcher Supporting Program funded by Korean Society of Cardiovascular Imaging (KOSCI) and the National Research Foundation of Korea (NRF) grant funded by the Korea government (MSIT) (No. 2021R1A2C4002195).

Acknowledgments

Medical Illustration & Design (MID), as a member of the Medical Research Support Services of Yonsei University College of Medicine, providing excellent support with medical illustration. The authors would like to thank Coreline Soft, Co., Ltd., for technical support.

REFERENCES

1. Detrano R, Guerci AD, Carr JJ, Bild DE, Burke G, Folsom AR, et al. Coronary calcium as a predictor of coronary events in four racial or ethnic groups. *N Engl J Med* 2008;358:1336-1345
2. Greenland P, LaBree L, Azen SP, Doherty TM, Detrano RC. Coronary artery calcium score combined with Framingham score for risk prediction in asymptomatic individuals. *JAMA* 2004;291:210-215
3. Arad Y, Goodman KJ, Roth M, Newstein D, Guerci AD. Coronary calcification, coronary disease risk factors, C-reactive protein, and atherosclerotic cardiovascular disease events: the St. Francis heart study. *J Am Coll Cardiol* 2005;46:158-165
4. Reiter MJ, Nemesure A, Madu E, Reagan L, Plank A. Frequency and distribution of incidental findings deemed appropriate for S modifier designation on low-dose CT in a lung cancer screening program. *Lung Cancer* 2018;120:1-6
5. Jacobs PC, Gondrie MJ, van der Graaf Y, de Koning HJ, Isgum I, van Ginneken B, et al. Coronary artery calcium can predict all-cause mortality and cardiovascular events on low-dose CT screening for lung cancer. *AJR Am J Roentgenol* 2012;198:505-511
6. Mets OM, Vliegenthart R, Gondrie MJ, Viergever MA, Oudkerk M, de Koning HJ, et al. Lung cancer screening CT-based prediction of cardiovascular events. *JACC Cardiovasc Imaging* 2013;6:899-907
7. Chiles C, Duan F, Gladish GW, Ravenel JG, Baginski SG, Snyder BS, et al. Association of coronary artery calcification and mortality in the national lung screening trial: a comparison of three scoring methods. *Radiology* 2015;276:82-90
8. Shemesh J, Henschke CI, Shaham D, Yip R, Farooqi AO, Cham MD, et al. Ordinal scoring of coronary artery calcifications on low-dose CT scans of the chest is predictive of death from cardiovascular disease. *Radiology* 2010;257:541-548
9. Phillips WJ, Johnson C, Law A, Turek M, Small AR, Dent S, et al. Comparison of Framingham risk score and chest-CT identified coronary artery calcification in breast cancer patients to predict cardiovascular events. *Int J Cardiol* 2019;289:138-143
10. Budoff MJ, Lutz SM, Kinney GL, Young KA, Hokanson JE, Barr RG, et al. Coronary artery calcium on noncontrast thoracic computerized tomography scans and all-cause mortality. *Circulation* 2018;138:2437-2438
11. Jacobs PC, Gondrie MJ, Mali WP, Oen AL, Prokop M, Grobbee DE, et al. Unrequested information from routine diagnostic chest CT predicts future cardiovascular events. *Eur Radiol* 2011;21:1577-1585
12. Shao L, Yan AT, Lebovic G, Wong HH, Kirpalani A, Deva DP. Prognostic value of visually detected coronary artery calcification on unenhanced non-gated thoracic computed tomography for prediction of non-fatal myocardial infarction and all-cause mortality. *J Cardiovasc Comput Tomogr* 2017;11:196-202
13. Osborne-Grinter M, Ali A, Williams MC. Prevalence and clinical implications of coronary artery calcium scoring on non-gated thoracic computed tomography: a systematic review and meta-analysis. *Eur Radiol* 2024;34:4459-4474
14. Hecht HS, Cronin P, Blaha MJ, Budoff MJ, Kazerooni EA, Narula J, et al. 2016 SCCT/STR guidelines for coronary artery calcium scoring of noncontrast noncardiac chest CT scans: a report of the Society of Cardiovascular Computed Tomography and Society of Thoracic Radiology. *J Cardiovasc Comput Tomogr* 2017;11:74-84
15. Dyer DS, White C, Conley Thomson C, Gieske MR, Kanne JP, Chiles C, et al. A quick reference guide for incidental findings on lung cancer screening CT examinations. *J Am Coll Radiol* 2023;20:162-172
16. Blaha MJ, Mortensen MB, Kianoush S, Tota-Maharaj R, Cainzos-Achirica M. Coronary artery calcium scoring: is it time for a change in methodology? *JACC Cardiovasc Imaging* 2017;10:923-937
17. Lessmann N, van Ginneken B, Zreik M, de Jong PA, de Vos BD, Viergever MA, et al. Automatic calcium scoring in low-dose chest CT using deep neural networks with dilated convolutions. *IEEE Trans Med Imaging* 2018;37:615-625
18. Martin SS, van Assen M, Rapaka S, Hudson HT Jr, Fischer AM, Varga-Szemes A, et al. Evaluation of a deep learning-based automated CT coronary artery calcium scoring algorithm. *JACC Cardiovasc Imaging* 2020;13(2 Pt 1):524-526
19. van Velzen SGM, Lessmann N, Velthuis BK, Bank IEM, van den Bongard DHJG, Leiner T, et al. Deep learning for automatic calcium scoring in CT: validation using multiple cardiac CT and chest CT protocols. *Radiology* 2020;295:66-79
20. Yang DH. Application of artificial intelligence to cardiovascular computed tomography. *Korean J Radiol* 2021;22:1597-1608
21. Lee JG, Kim H, Kang H, Koo HJ, Kang JW, Kim YH, et al. Fully automatic coronary calcium score software empowered by artificial intelligence technology: validation study using three CT cohorts. *Korean J Radiol* 2021;22:1764-1776

22. Kang HW, Ahn WJ, Jeong JH, Suh YJ, Yang DH, Choi H, et al. Evaluation of fully automated commercial software for Agatston calcium scoring on non-ECG-gated low-dose chest CT with different slice thickness. *Eur Radiol* 2023;33:1973-1981
23. Suh YJ, Kim C, Lee JG, Oh H, Kang H, Kim YH, et al. Fully automatic coronary calcium scoring in non-ECG-gated low-dose chest CT: comparison with ECG-gated cardiac CT. *Eur Radiol* 2023;33:1254-1265
24. Park S, Lee SM, Do KH, Lee JG, Bae W, Park H, et al. Deep learning algorithm for reducing CT slice thickness: effect on reproducibility of radiomic features in lung cancer. *Korean J Radiol* 2019;20:1431-1440
25. Bak SH, Kim JH, Jin H, Kwon SO, Kim B, Cha YK, et al. Emphysema quantification using low-dose computed tomography with deep learning-based kernel conversion comparison. *Eur Radiol* 2020;30:6779-6787
26. Tanabe N, Kaji S, Shima H, Shiraishi Y, Maetani T, Oguma T, et al. Kernel conversion for robust quantitative measurements of archived chest computed tomography using deep learning-based image-to-image translation. *Front Artif Intell* 2022;4:769557
27. Park H, Hwang EJ, Goo JM. Deep learning-based kernel adaptation enhances quantification of emphysema on low-dose chest CT for predicting long-term mortality. *Invest Radiol* 2024;59:278-286
28. Choi H, Kim H, Jin KN, Jeong YJ, Chae KJ, Lee KH, et al. A challenge for emphysema quantification using a deep learning algorithm with low-dose chest computed tomography. *J Thorac Imaging* 2022;37:253-261
29. Kang SJ, Kim YH, Lee JG, Kang DY, Lee PH, Ahn JM, et al. Impact of subtended myocardial mass assessed by coronary computed tomographic angiography-based myocardial segmentation. *Am J Cardiol* 2019;123:757-763
30. Vonder M, Zheng S, Dorrius MD, van der Aalst CM, de Koning HJ, Yi J, et al. Deep learning for automatic calcium scoring in population-based cardiovascular screening. *JACC Cardiovasc Imaging* 2022;15:366-367
31. Viscarra Rossel RA, Hicks WS. Soil organic carbon and its fractions estimated by visible–near infrared transfer functions. *Eur J Soil Sci* 2015;66:438-450
32. Rumberger JA, Sheedy PF 2nd, Breen JF, Fitzpatrick LA, Schwartz RS. Electron beam computed tomography and coronary artery disease: scanning for coronary artery calcification. *Mayo Clin Proc* 1996;71:369-377
33. Morsbach F, Berger N, Desbiolles L, Poropat T, Leschka S, Alkadhi H, et al. Systematic analysis on the relationship between luminal enhancement, convolution kernel, plaque density, and luminal diameter of coronary artery stenosis: a CT phantom study. *Int J Cardiovasc Imaging* 2013;29:1129-1135
34. Neubauer J, Spira EM, Strube J, Langer M, Voss C, Kotter E. Image quality of mixed convolution kernel in thoracic computed tomography. *Medicine (Baltimore)* 2016;95:e5309
35. An S, Fan R, Zhao B, Yi Q, Yao S, Shi X, et al. Evaluating coronary artery calcification with low-dose chest CT reconstructed by different kernels. *Clin Imaging* 2022;83:166-171
36. Mühlenbruch G, Thomas C, Wildberger JE, Koos R, Das M, Hohl C, et al. Effect of varying slice thickness on coronary calcium scoring with multislice computed tomography in vitro and in vivo. *Invest Radiol* 2005;40:695-699
37. van Assen M, Martin SS, Varga-Szemes A, Rapaka S, Cimen S, Sharma P, et al. Automatic coronary calcium scoring in chest CT using a deep neural network in direct comparison with non-contrast cardiac CT: a validation study. *Eur J Radiol* 2021;134:109428
38. Choi JH, Cha MJ, Cho I, Kim WD, Ha Y, Choi H, et al. Validation of deep learning-based fully automated coronary artery calcium scoring using non-ECG-gated chest CT in patients with cancer. *Front Oncol* 2022;12:989250
39. Xu J, Liu J, Guo N, Chen L, Song W, Guo D, et al. Performance of artificial intelligence-based coronary artery calcium scoring in non-gated chest CT. *Eur J Radiol* 2021;145:110034
40. Park C, Lee BC, Jeong WG, Park WJ, Jin GY, Kim YH. Coronary artery calcification on low-dose lung cancer screening CT in South Korea: visual and artificial intelligence-based assessment and association with cardiovascular events. *AJR Am J Roentgenol* 2024;222:e2430852
41. Fan R, Shi X, Qian Y, Wang Y, Fan L, Chen R, et al. Optimized categorization algorithm of coronary artery calcification score on non-gated chest low-dose CT screening using iterative model reconstruction technique. *Clin Imaging* 2018;52:287-291
42. Szilveszter B, Elzomor H, Károlyi M, Kolossváry M, Raaijmakers R, Benke K, et al. The effect of iterative model reconstruction on coronary artery calcium quantification. *Int J Cardiovasc Imaging* 2016;32:153-160
43. Wang Y, Zhan H, Hou J, Ma X, Wu W, Liu J, et al. Influence of deep learning image reconstruction and adaptive statistical iterative reconstruction-V on coronary artery calcium quantification. *Ann Transl Med* 2021;9:1726
44. Oda S, Utsunomiya D, Nakaura T, Funama Y, Yuki H, Kidoh M, et al. The influence of iterative reconstruction on coronary artery calcium scoring—phantom and clinical studies. *Acad Radiol* 2017;24:295-301
45. Kronmal RA, McClelland RL, Detrano R, Shea S, Lima JA, Cushman M, et al. Risk factors for the progression of coronary artery calcification in asymptomatic subjects: results from the multi-ethnic study of atherosclerosis (MESA). *Circulation* 2007;115:2722-2730
46. Bailey G, Healy A, Young BD, Sharma E, Meadows J, Chun HJ, et al. Relative predictive value of lung cancer screening CT versus myocardial perfusion attenuation correction CT in the evaluation of coronary calcium. *PLoS One* 2017;12:e0175678
47. Christensen JL, Sharma E, Gorvitovskaia AY, Watts JP Jr, Assali M, Neverson J, et al. Impact of slice thickness on the predictive value of lung cancer screening computed tomography in the evaluation of coronary artery calcification. *J Am Heart Assoc* 2019;8:e010110

https://doi.org/10.3348/kjr.2025.0177